

General many-body entanglement swapping protocol

Santeri Huhtanen,^{1,2} Yousef Mafi,^{1,2} Ali G. Moghaddam,^{1,2,3,*} and Teemu Ojanen^{1,2,†}

¹Computational Physics Laboratory, Physics Unit, Faculty of Engineering and Natural Sciences, Tampere University, P.O. Box 692, FI-33014 Tampere, Finland

²Helsinki Institute of Physics P.O. Box 64, FI-00014, Finland

³Department of Applied Physics, Aalto University, 02150 Espoo, Finland

(Dated: June 30, 2025)

Sharing entangled pairs between non-signaling parties via entanglement swapping constitutes a striking demonstration of the nonlocality of quantum mechanics and a crucial building block for future quantum technologies. In this work, we generalize pair-swapping methods by introducing a many-body entanglement swapping protocol, which allows two non-signaling parties to share general many-body states along an arbitrary partitioning. The shared many-body state retains exactly the same Schmidt vectors as the target state and exhibits typically high fidelity, which approaches unity as the variance of the Schmidt coefficients vanishes. The cost of many-body swapping—arising from postselection in a third-party measurement—is determined by the 3rd Rényi entanglement entropy of the partitioning. We provide a proof of concept of the protocol on real quantum hardware and discuss how it enables new functionalities, such as flexible sharing of complex multi-qubit states and fault-tolerant entanglement swapping.

I. INTRODUCTION

The ability to share quantum states nonlocally—across distances ranging from microns to hundreds of kilometers—is one of the most intriguing features of quantum mechanics. At the same time, it plays a central role in enabling practical tasks in quantum information processing, particularly in distributed systems and quantum networks [1, 2]. One powerful protocol for achieving long-range quantum information transfer is *entanglement swapping*, which allows two distant, non-signaling parties to share an entangled state through the use of intermediate entangled pairs [3, 4]. This counterintuitive phenomenon highlights the fundamentally nonlocal character of quantum mechanics and represents a clear departure from classical intuition [5–7]. Beyond its conceptual significance, entanglement swapping has become a key tool in the development of quantum repeaters, quantum communication architectures, and foundational tests of quantum mechanics [8–13].

In addition to long-distance applications, the ability to share quantum states over short distances is equally critical for quantum computing—especially as we look beyond the Noisy Intermediate-Scale Quantum (NISQ) era. This current era has been constrained by limited qubit counts, high error rates, and sparse hardware connectivity [14–17]. Looking ahead, the envisioned “megaquop” era anticipates quantum processors capable of reliably performing on the order of one million operations [18]. In this context, the need for robust and scalable methods to generate and control complex entanglement across distant qubits becomes even more pressing. Such capabilities support not only nonlocal multi-qubit

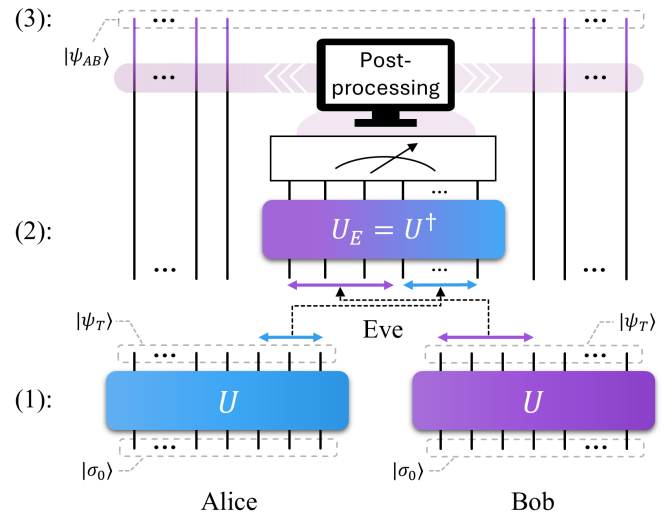


FIG. 1. Many-body entanglement swapping protocol. In step 1, Alice and Bob create locally a target state $|\psi_T\rangle = U|\sigma_0\rangle$ which determines the entanglement structure of the shared state. They share the state along partition in which Alice holds n_A and Bob holds n_B qubits respectively, and send the remaining qubits to Eve. In step 2, Eve applies unitary U_E to her qubits and then measures them. If she obtains result $|\sigma_0\rangle$, she informs Alice and Bob to keep their qubits, otherwise discard them. In step 3, after postselection, Alice and Bob share entangled state $|\psi_{AB}\rangle$ which share exactly the same Schmidt eigenstates as $|\psi_T\rangle$ and simply related Schmidt coefficients λ_i^{AB} .

gates—essential for advanced algorithms and quantum error correction [19]—but also play a foundational role in quantum simulation [20], distributed computing models, and the development of large-scale quantum supercomputers [21].

In this work, we introduce a many-body entanglement-swapping protocol which generalizes pair-swapping meth-

* Email: ali.moghaddam@aalto.fi

† Email: teemu.ojanen@tuni.fi

ods and enables flexible, high-fidelity sharing of complex multi-qubit states $|\psi_{AB}\rangle$. As illustrated in Fig. 1, the protocol proceeds in three stages. First, Alice and Bob each generate the target state $|\psi_T\rangle$ with a unitary U , retain the qubits corresponding to their respective partitions, and transmit the remaining qubits to an intermediary party, Eve. In the second stage, Eve applies the inverse unitary U^\dagger to the received qubits, performs a projective measurement, and broadcasts the outcome to Alice and Bob. When Eve's measurement yields a desired result, Alice and Bob's joint state collapses to $|\psi_{AB}\rangle$, which shares exactly the same Schmidt vectors as $|\psi_T\rangle$, and whose Schmidt coefficients are simply related to those of the target state. We show that the fidelity of the shared states is typically high—even for complex many-body states—and becomes unity when the Schmidt spectrum is uniform. The fundamental cost of the swapping, characterized by the postselection probability in Eve's measurement, is determined by the 3rd Rényi entanglement entropy of the partitioning. We demonstrate the proof of principle of our protocol in real quantum hardware and explain how it allows fault-tolerant quantum state sharing between non-signaling parties.

The many-body swapping protocol, enabling a reliable sharing of complex entangled states, opens new avenues for scalable quantum networks and distributed quantum information processing. Particularly, while recent advances in dynamic quantum circuits, featuring mid-circuit measurements and real-time feed-forward, have enabled the teleportation of two-qubit gates across large superconducting arrays [22–24], these approaches are mostly effective for low-complexity states and become increasingly inefficient for more intricate entanglement structures. In contrast, our many-body swapping protocol addresses these limitations by offering a scalable and hardware-efficient strategy for entanglement distribution, which is essential for the mequop era and large-scale quantum technologies.

II. MANY-BODY ENTANGLEMENT SWAPPING PROTOCOL

In this section we outline our many-body entanglement swapping protocol. We search for a method that would, on one hand, allow two non-signaling parties Alice and Bob to share a target many-body state $|\psi_T\rangle$, which they can generate locally, along an arbitrary partitioning. On the other hand, not counting the usual practical limitations of carrying out unitary transformations and measurements, the protocol should be explicit and straightforwardly applicable. While the ability to share a state precisely and straightforwardly are competing demands, below we see that it is possible to reconcile with the requirement to an impressive degree. We identify a large class of systems where the sharing can be done exactly or with high accuracy, and even when that is not the case, the entanglement structure of the shared state is

straightforwardly inherited from the target state.

The general protocol is agnostic to the precise nature of the elementary degrees of freedom (qubits, qudits etc), but for the sake of concreteness, we consider a system of qubits. Assume that two parties, Alice and Bob, can locally prepare a target multi-qubit state

$$|\psi_T\rangle = U|\sigma_0\rangle, \quad (1)$$

where U is unitary acting on n qubits and $|\sigma_0\rangle$ denotes a product state in the computational basis. Now, Alice and Bob would like to share $|\psi_T\rangle$ along an arbitrary partitioning in such a way that Alice is in possession of a set of qubits $\{N_A\}$ with n_A elements, spanning the Hilbert space \mathcal{H}_A . Bob, on the other hand, should be in the possession of the remaining set $\{N_B\}$ with $n_B = n - n_A$ elements, spanning the Hilbert space \mathcal{H}_B . Furthermore, the protocol should be carried out without signaling between Alice and Bob, but with a help of a third party, Eve, as illustrated in Fig. 1.

In the first step, both parties prepare locally the target state. Thus, the initial state becomes

$$|\Psi_1\rangle = |\psi_T\rangle \otimes |\psi_T\rangle,$$

where $|\psi_T\rangle \in \mathcal{H}_A \otimes \mathcal{H}_B$. Considering a bipartitioning into subsystems $\{N_A\}$ and $\{N_B\}$, the Schmidt decomposition of the target state can be written as

$$|\psi_T\rangle = \sum_i \sqrt{\lambda_i} |\lambda_i^A\rangle \otimes |\lambda_i^B\rangle, \quad (2)$$

where $\lambda_i > 0$ are the Schmidt coefficients and $|\lambda_i^A\rangle \in \mathcal{H}_A$, $|\lambda_i^B\rangle \in \mathcal{H}_B$ are the orthonormal Schmidt vectors corresponding to the partitioning. Using this, we can express the initial state of the two parties as

$$|\Psi_1\rangle = \sum_{i,j} \sqrt{\lambda_i \lambda_j} |\lambda_i^A\rangle \otimes |\lambda_i^B\rangle \otimes |\lambda_j^A\rangle \otimes |\lambda_j^B\rangle.$$

In the second step, Alice sends her set of qubits $\{N_B\}$ and Bob his set $\{N_A\}$ to Eve, who will then apply a unitary U_E on her qubits, leading to state $|\Psi_2\rangle = U_E|\Psi_1\rangle$. This can be expressed as

$$|\Psi_2\rangle = \sum_{i,j} \sqrt{\lambda_i \lambda_j} |\lambda_i^A\rangle \otimes U_E(|\lambda_i^B\rangle \otimes |\lambda_j^A\rangle) \otimes |\lambda_j^B\rangle.$$

Then, Eve measures all her qubits in the computational basis $\{|\sigma_i\rangle\}$. Assuming the measurement outcome is $|\sigma_E\rangle$, the final state becomes

$$\begin{aligned} |\Psi_3\rangle &= \frac{1}{\sqrt{p_E}} (\mathbb{1} \otimes |\sigma_E\rangle) \langle \sigma_E | \otimes \mathbb{1} | \Psi_2 \rangle \\ &= \frac{1}{\sqrt{p_E}} \sum_{i,j} \sqrt{\lambda_i \lambda_j} r_{ij}^E |\lambda_i^A\rangle \otimes |\sigma_E\rangle \otimes |\lambda_j^B\rangle, \end{aligned}$$

where the coefficients r_{ij}^E are

$$r_{ij}^E \equiv \langle \sigma_E | U_E (|\lambda_i^B\rangle \otimes |\lambda_j^A\rangle),$$

and the probability of outcome $|\sigma_E\rangle$ is given by

$$p_E = \sum_{i,j} \lambda_i \lambda_j |r_{ij}^E|^2. \quad (3)$$

As the final state has a product form with respect to Eve, her state can be trivially factored out. Thus, we can focus on the joint n qubit state for which Alice holds n_A and Bob n_B qubits:

$$|\psi_{AB}\rangle = \frac{1}{\sqrt{p_E}} \sum_{i,j} \sqrt{\lambda_i \lambda_j} r_{ij}^E |\lambda_i^A\rangle \otimes |\lambda_j^B\rangle.$$

The joint state of Alice and Bob depends on Eve's measurement outcome $|\sigma_E\rangle$ in the last step, which is non-deterministic. This fact, in general, necessitates postselection, which can be avoided in special cases. The overlap of the target state and the state resulting from the many-body swapping becomes

$$F = \langle \psi_T | \psi_{AB} \rangle = \frac{1}{\sqrt{p_E}} \sum_k \lambda_k^{3/2} r_{kk}^E, \quad (4)$$

providing an important figure of merit $|F|$ called fidelity, which satisfies $0 \leq |F| \leq 1$. Ideally, one would like $|F|$ to be as close to unity as possible while satisfying the constraint $\sum_{ij} |r_{ij}^E|^2 \leq 1$. Optimal solutions clearly satisfy $r_{ij}^E = r_{ii} \delta_{ij}$ and all r_{ii} should have the same complex phase. These two conditions now suggest an efficient strategy for Eve to choose her unitary U_E and the post-selected state. In above, we assumed that U_E is acting in the Hilbert space $\mathcal{H}_B \otimes \mathcal{H}_A$, but it is now convenient to work in the reordered basis $\mathcal{H}_A \otimes \mathcal{H}_B$, where the corresponding unitary is denoted as U'_E . The two representations are related so that $U_E(|\lambda_i^B\rangle \otimes |\lambda_i^A\rangle)$ in the basis $\mathcal{H}_B \otimes \mathcal{H}_A$ corresponds to the vector $U'_E(|\lambda_i^A\rangle \otimes |\lambda_i^B\rangle)$ in the basis $\mathcal{H}_A \otimes \mathcal{H}_B$ for all vectors $|\lambda_i^A\rangle \in \mathcal{H}_A$ and $|\lambda_i^B\rangle \in \mathcal{H}_B$. Combining Eqs. (1), (2), we see that

$$U|\sigma_0\rangle = \sum_i \sqrt{\lambda_i} |\lambda_i^A\rangle \otimes |\lambda_i^B\rangle.$$

Thus, if Eve chooses $U'_E = U^\dagger$ and postselects to retain only the measurement outcomes for which $|\sigma_E\rangle = |\sigma_0\rangle$, we see that $r_{ij}^E = \sqrt{\lambda_i} \delta_{ij}$ and $r_{ii} > 0$. The fidelity then becomes

$$F = \frac{\sum_k \lambda_k^2}{\sqrt{\sum_m \lambda_m^3}} = e^{S_3(\{\lambda_i\}) - S_2(\{\lambda_i\})}, \quad (5)$$

where we have employed Rényi entropies

$$S_n(\{\lambda_i\}) = \frac{1}{1-n} \ln \sum_i \lambda_i^n.$$

After the swapping protocol, the shared state itself becomes

$$|\psi_{AB}\rangle = \sum_i \sqrt{\lambda_i^{AB}} |\lambda_i^A\rangle \otimes |\lambda_i^B\rangle, \quad (6)$$

which has the exact same Schmidt vectors than the target state. The Schmidt coefficients of the shared state are simply given in terms of the target state coefficients as

$$\lambda_i^{AB} = \frac{\lambda_i^3}{\sum_m \lambda_m^3}. \quad (7)$$

The probability (3) of obtaining the desired outcome state $|\sigma_0\rangle$ in Eve's measurement in turn becomes

$$p_0 = \sum_i \lambda_i^3 = e^{-2S_3(\{\lambda_i\})}. \quad (8)$$

This probability is also the success rate for the postselection and characterizes the mean number of trials $\sim 1/p_0$ to share a single copy of $|\psi_{AB}\rangle$ between Alice and Bob.

A few observations are in order. The overlap (5) of the shared and the target state becomes unity when $S_2(\{\lambda_i\}) = S_3(\{\lambda_i\})$, which happens when the Schmidt spectrum is uniform $\lambda_i = \lambda_j$ for all i, j . This case covers, as special cases, maximum entropy states, GHZ-type states, various cluster states (for simple partitionings) and a large class of other possibilities. Importantly, the overlap often remains very high even for non-uniform spectrum. To see this, it is useful to parameterize the Schmidt coefficients as $\lambda_i = d_S^{-1} + \epsilon_i$, where d_S is the Schmidt rank (the number of nonzero Schmidt coefficients) and ϵ_i is the deviation from the mean value. The fidelity (5) then becomes

$$F = \frac{1 + d_S^2 \bar{\epsilon}^2}{\sqrt{1 + 3d_S^2 \bar{\epsilon}^2 + d_S^3 \bar{\epsilon}^3}} \xrightarrow{\bar{\epsilon}^2 \rightarrow 0} 1 - \frac{d_S^2 \bar{\epsilon}^2}{2} + \mathcal{O}(d_S^3 \bar{\epsilon}^3),$$

where $\bar{\epsilon}^n = d_S^{-1} \sum_i \epsilon_i^n$ for $n = 2, 3$ determine the variance and the skewness of the Schmidt coefficients. Thus, the overlap remains nearly perfect whenever the non-uniformity satisfies $d_S^2 \bar{\epsilon}^2 \ll 1$. Even for significant non-uniformity $d_S^2 \bar{\epsilon}^2, d_S^3 \bar{\epsilon}^3 \sim 1$, the fidelity remains remarkably high $F \sim 2/\sqrt{5} \sim 0.9$. Below we illustrate how complex multi-qubit random states can be shared with comparable fidelity. In addition, irrespective of the fidelity, the entanglement structure of the shared state is always inherited from the target state, with exactly coinciding Schmidt vectors and the Schmidt coefficients that are related to those of the target state by Eq. (7). Therefore, the protocol enables an explicit method of sharing a known many-body state with a close resemblance to a general target state.

Finally, the fundamental cost of the many-body swapping is determined by the success probability (8) of postselection. The lower the probability, the more repetitions are required for sharing a single copy of $|\psi_{AB}\rangle$. Importantly, the cost *does not* depend explicitly on the number of qubits in the shared state, but only on the entanglement entropy S_3 of the partitioning. Thus, the fundamental protocol complexity does not directly depend on the system size, but only on the shared entanglement. For example, many interesting one-dimensional

condensed-matter phases and their quantum circuit representations exhibit an area-law entanglement entropy scaling [25, 26]. This means that the entanglement entropy of partitioning does not depend on the total system size, so the cost of sharing them would also be size independent. The same conclusion also holds for 1d states generated by *sequential quantum circuits* capable of generating area-law entangled states with complex internal structure, including GHZ states and various topologically ordered states [27, 28]. In some simple cases, as discussed below, it is possible to avoid postselection simply by applying local unitaries to correct the shared state, as in the pair swapping.

III. EXAMPLES OF MANY-BODY SWAPPING

Here we illustrate the general many-body entanglement swapping protocol with examples. To set the stage, we provide a proof of concept of the protocol in real quantum hardware by sharing multi-qubit GHZ states. While this outcome could be accomplished by a standard Bell pair swapping and local operations, this example shows that the many-body protocol is robust to imperfections in the present quantum hardware. In Sec. IV B this example is also used to illustrate how the many-body protocol can readily implement quantum error correction and fault-tolerant swapping. The true versatility of the many-body swapping protocol, however, becomes evident when addressing general problems of sharing arbitrary many-body entangled states with non-uniform Schmidt spectra. In such cases, pair-swapping approaches become impractical, and the many-body protocol offers efficient alternative.

A. Proof of concept on quantum hardware

Here we consider the task of distributing an n -qubit GHZ state between two parties, Alice and Bob. The target state is given by

$$|\psi_T\rangle = \frac{1}{\sqrt{2}}(|00\dots 0\rangle + |11\dots 1\rangle), \quad (9)$$

where Alice and Bob initially each hold n qubits and can perform arbitrary operations on their respective systems. To implement the protocol, both parties must locally prepare an n -qubit GHZ state. This is achievable from the initial state $|00\dots 0\rangle$ by a quantum circuit composed of a Hadamard gate followed by a series of CNOT gates, as shown in Fig. 2(a). The goal of the many-body entanglement swapping is to generate a shared GHZ state between n_A qubits on Alice's side and $n_B = n - n_A$ qubits on Bob's side, while transferring the remaining qubits to an intermediary, Eve. Following the general procedure outlined in Fig. 1, Eve applies a basis-reordered inverse unitary operation to the qubits received from Alice and

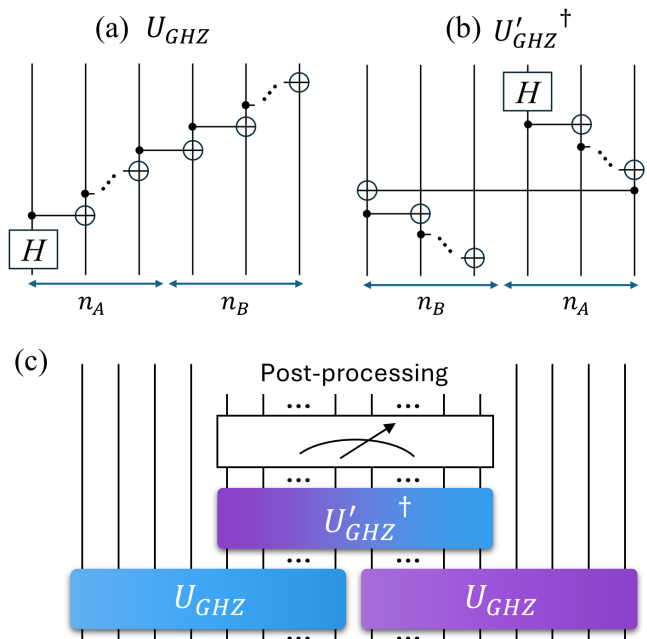


FIG. 2. (a) Circuit for preparing GHZ states. (b) Inverse unitary in the basis where the order of Alice and Bob qubits are switched. (c) Protocol for creating a shared GHZ state for the outermost qubits.

Bob, illustrated in Fig. 2(b). The full circuit implementation of the protocol is shown in Fig. 2(c). Upon completing her operation, Eve measures her qubits. The possible outcomes are

$$\{|00\dots 0\rangle, |00\dots, 11\dots\rangle, |11\dots, 00\dots\rangle, |11\dots 1\rangle\},$$

each occurring with probability $1/4$. If the result is $|00\dots 0\rangle$, the resulting state shared between Alice and Bob matches the target GHZ state $|\psi_T\rangle$, with Alice holding the first n_A qubits. Interestingly, even the other measurement outcomes lead to GHZ-like entangled states, differing from $|\psi_T\rangle$ only by local bit-flip operations. This means postselection is not necessary: Alice and Bob can always recover the target state by applying appropriate local corrections.

To demonstrate a proof of concept for our many-body entanglement-swapping protocol under realistic conditions, we implemented GHZ state sharing using IBM's superconducting quantum hardware [29]. The protocol was executed for systems of up to 12 qubits, enabling the sharing of GHZ states with up to 6 qubits (see Methods, Subsec. XI A, for details of the simulations on real hardware). The results are summarized in Fig. 3, which includes both experimental outcomes and corresponding simulations incorporating realistic noise models. Figures 3(a) and (b) display the experimentally measured output distributions for Alice and Bob's qubits in GHZ states of $n = 2$ and $n = 3$ qubits, respectively. The observed bit-string frequencies exhibit the characteristic correlations of GHZ states, confirming the expected entanglement structure. Figure 3(c)

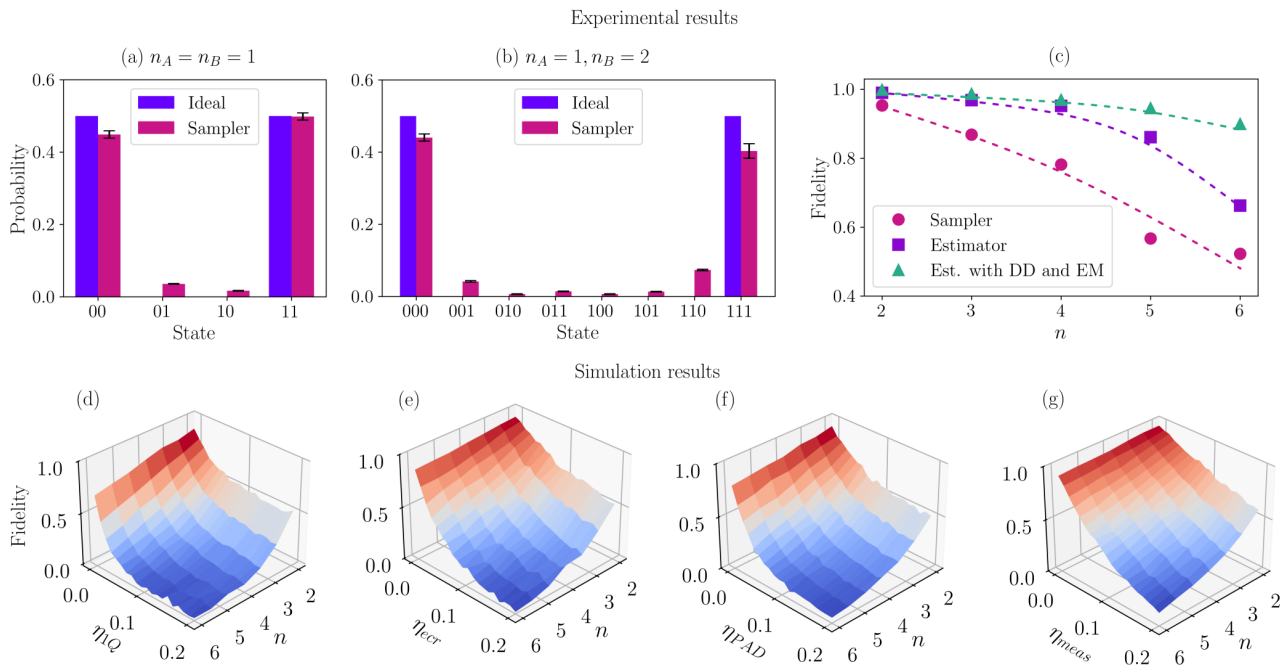


FIG. 3. (a–b) Vector state probability distributions for 2- and 3-qubit GHZ states obtained using the Sampler method. The error bars represent the standard deviation. (c) GHZ state fidelity as a function of qubit number for three different approaches: (1) Sampler, (2) Estimator, and (3) Estimator with dynamical decoupling (DD) and error mitigation (EM). (d–g) Simulated fidelity decay of GHZ states as a function of qubit number under various noise sources: (d) single-qubit gate errors, (e) ECR gate errors, (f) phase-amplitude damping, and (g) readout errors. See Methods, Subsec. XI A, for detailed descriptions of the Sampler and Estimator methods and the noise models used in the simulations.

presents the fidelity of the shared target state as a function of the number of qubits, comparing results obtained from the quantum hardware using three different measurement approaches: (i) the *Sampler*, which records raw bitstring outcomes without post-processing; (ii) the *Estimator*, which computes expectation values of observables using shot optimization and standard error mitigation techniques; and (iii) the *Estimator* combined with additional post-processing, including dynamical decoupling and enhanced error mitigation strategies. This comparison isolates the contribution of hardware-induced errors, demonstrating that standard error mitigation techniques can recover fidelity levels close to the performance ceiling imposed by the physical device.

Panels (d–g) of Fig. 3 present the simulated fidelity degradation as a function of qubit number under varying strengths of different noise sources, including single-qubit gate errors, two-qubit ECR gate errors, phase-amplitude damping, and readout errors (see Methods, Subsec. XIB for noise model details). These results identify the dominant noise mechanisms and provide valuable insight into the protocol’s scalability and robustness under realistic conditions. Overall, the data confirm that the many-body swapping protocol can be implemented with good fidelity on existing quantum hardware. Furthermore, as discussed in Sec. IV B, the protocol is compatible with standard quantum error correction techniques, allowing for a fault-tolerant implementation of entanglement

swapping.

B. Sharing entangled states with non-uniform Schmidt spectra

We now consider sharing target states with non-uniform Schmidt spectrum. This class of states poses a challenge for pair-swapping methods and highlights the applicability of the many-body protocol. As a concrete example, we consider a four-qubit target state of the form $|\psi_T\rangle = U|0000\rangle$, generated by some unitary transformation U , where Alice and Bob each hold two qubits. The Schmidt rank for this bipartition is $d_S = 2^2 = 4$, and the state is generally characterized by four distinct Schmidt coefficients $\{\lambda_i\}$ with $i = 1, \dots, 4$.

To share such a state using the many-body protocol, we consider a representative case where the Schmidt coefficients are chosen as $\{\lambda_i\} = \{0.4, 0.3, 0.2, 0.1\}$. In this instance, the fidelity between the target state $|\psi_T\rangle$ and the shared state of Alice and Bob, denoted $|\psi_{AB}\rangle$, is found to be $F = \langle \psi_T | \psi_{AB} \rangle = 0.95$, as given by Eq. (5). The Schmidt coefficients of the resulting shared state, computed using Eq. (7), are $\{\lambda_i^{AB}\} = \{0.64, 0.27, 0.08, 0.01\}$, indicating a distortion from the original spectrum. According to Eq. (8), the probability of successful postselection in this example is $p_0 = 0.1$. This implies that, on average, the protocol must be repeated approximately ten

times to successfully share a single copy of $|\psi_{AB}\rangle$. While the shared state does not match the target exactly, the high fidelity underscores the protocol's effectiveness. A high fidelity can persist even for much larger and more complex states, as seen in the following example.

C. Sharing multi-qubit states generated by random unitary circuits

Next we illustrate how the many-body swapping protocol enables high-fidelity sharing of complex, high-entropy quantum states. In particular, we focus on target states generated by random two-qubit brickwork circuits, as depicted in Fig. 4(b). Such circuits have become widely used as testbeds for exploring a range of many-body quantum phenomena, especially in the study of entanglement dynamics and information scrambling [30–32]. In the model considered here, the time-evolution operator for each cycle is defined as

$$\mathbf{u}(t) = \prod_{\text{even } l} u_{l,l+1}(2t) \prod_{\text{odd } l} u_{l,l+1}(2t-1),$$

where $u_{l,l+1}(\tau)$ denotes a two-qubit unitary acting on neighboring qubits l and $l+1$ at the discrete time step $\tau = 2t$ or $2t-1$. Each two-qubit gate is generated as

$$u_{l,l+1}(t) = e^{i(\phi_x X_l X_{l+1} + \phi_y Y_l Y_{l+1} + \phi_z Z_l Z_{l+1})},$$

where X_l , Y_l , and Z_l are the Pauli operators on qubit l , and the coefficients ϕ_i are independent random variables uniformly sampled from the interval $[-\pi, \pi]$. These random parameters are independently drawn for each gate location and time step. This ensemble of unitaries does not sample from the full Haar measure over two-qubit unitaries. However, the brick circuits generate maximum entropy states, up to finite-size corrections. Notably, when acting on an initial product state, these circuits rapidly generate entanglement across subsystems. After order of $T \sim n_s$ layers, where n_s is the number of qubits in the shared state, the entanglement entropy saturates close to the maximal value, scaling as $S_{n_s}/(n_s \ln 2) \sim 1 + \mathcal{O}(1/n_s)$. The fact that the random brickwork circuits generate nearly maximally entangled states has attracted significant interest in the past decade. Below we see that the highly scrambled, complex quantum states produced by such circuits can be shared by the many-body swapping protocol with high fidelity.

As seen in Fig. 4, for deep circuits ($T = T_{\max} \gtrsim 2n$) the average fidelity of the shared state, given by Eq. (5), is strikingly high. As the total system size increases from $n = 4$ to $n = 18$, the fidelity stays around $F = 0.9$. This is quite remarkable, given the complexity of these nearly maximum entropy states. However, as seen in Fig. 4 (c), the state sharing is exponentially costly in the system size, as the success probability for postselection is determined by the 3rd Rényi entropy through

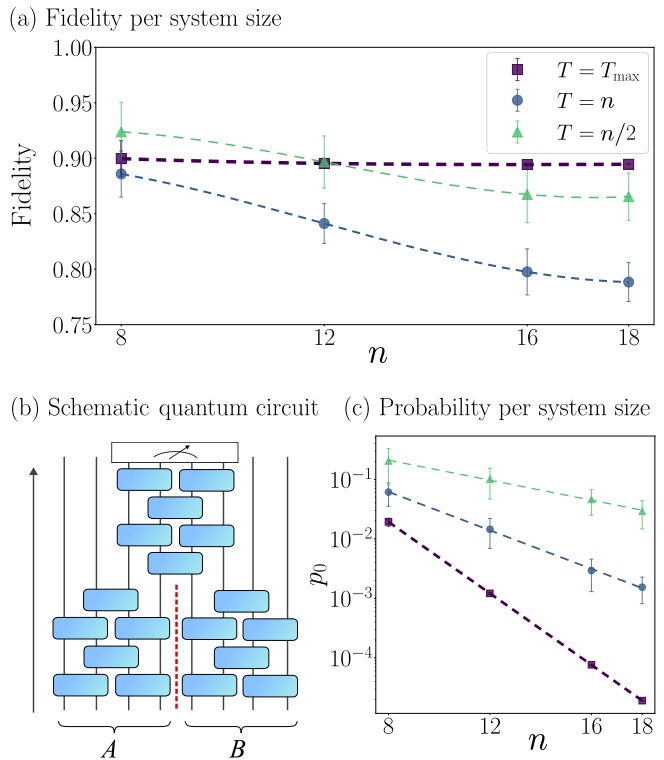


FIG. 4. Sharing states generated by a random unitary circuit: (a) The average fidelity (overlap of the shared state with the target state) given by expression (5) as a function of the system size n for random two-qubit brickwork circuits. (b) Schematic illustration of the random unitary circuit generating the target state shared between Alice and Bob. (c) The postselection probability of obtaining the desired shared state as a function of the system size.

Eq. (8). For highly entangled states approaching maximal entropy, the postselection probability scales approximately as $p_0 \approx 2^{-n}$. For instance, successfully sharing of a single $n = 18$ state (split evenly between two parties) would require on average 2.6×10^5 repetitions. This example highlights the substantial resource overhead associated with distributing highly entangled, high-entropy quantum states. Still, sharing smaller states $n \leq 10$ would require less than 10^3 repetitions on average.

IV. DISCUSSION

Here we highlight two crucial advantages of the many-body swapping protocol in comparison to the existing entanglement swapping methods.

A. Quantum state sharing with the many-body protocol versus pair swapping

Here we make the case why the many-body swapping protocol provides more practical approach for high-

fidelity sharing of general target states between non-signaling parties compared to the existing pair-based swapping methods. In the pair-based approaches, Alice and Bob aim to share a general n -qubit target state, where each party ends up holding $n/2$ qubits. They begin with a number of shared (maximally or partially) entangled pairs and the ability to perform local operations.

To understand the practical limitations of the pair-swapping methods, we note that upon bipartitioning a generic target state between Alice and Bob, the number of different Schmidt values is bounded by the Schmidt rank as $d_S - 1$, hence, can be as large as $2^{n/2} - 1$. Since local unitary operations preserve the Schmidt coefficients, and local measurements cannot independently adjust them, achieving a target state with N_{ind} distinct Schmidt coefficients would require access to at least N_{ind} entangled pairs—each carefully prepared with a unique, precisely tuned Schmidt coefficient. However, as pointed out above, for a generic many-qubit state, N_{ind} grows exponentially with the number of qubits and reaches up to $2^{n/2} - 1$. This implies that an exponentially large number of shared pair states would be needed, each tailored to contribute to a different component of the target state’s entanglement structure. Moreover, even if such a resource were available, one would still face the profound problem of determining the local operations which map the collection of entangled pairs to the target state. In general, these local operations are a priori unknown and state specific.

Due to these challenges, there is currently no known protocol based on pair-swapping that can reliably generate even a few-body target states with a generic Schmidt spectrum. In contrast, the many-body entanglement swapping protocol introduced in this work is explicit, straightforward to implement, and leads directly to a shared state with the correct Schmidt vectors and typically high fidelity. Thus, given the formidable practical challenges associated with pair-swapping approaches, the many-body protocol stands out as an attractive and feasible method for sharing general entangled states between non-signaling parties.

B. Error correction and fault-tolerant entanglement swapping

The simple GHZ state sharing example in Sec. III A suggests an interesting application of the many-body swapping. While a shared GHZ could be generated by a single swapped Bell pair and local operations, the many-body protocol has an important advantage. Let’s consider, for example, a realistic scenario in which Eve’s measurement process is unideal. In that case, she has a small but finite probability p^* of registering a wrong outcome from a measurement process of a single qubit. In pair swapping-based schemes, a single error in the swapping measurement propagates to the shared GHZ state and contaminates it with the same probability p^* . On

the other hand, in the many-body swapping protocol, Alice and Bob send multiple qubits to Eve and a single error in the measurement process can be detected. For instance, instead of obtaining a correct outcome $|0000\dots1111\rangle$, Eve could in fact register an erroneous outcome $|0000\dots1101\rangle$, where a single bit has flipped. Despite the error, Eve has no difficulties in identifying the state correctly and communicating the right result to Alice and Bob.

The error detection example above reflects the fact that a GHZ state can be regarded as a Bell state formed by logical qubits which are encoded by a simple repetition code $|0\rangle \rightarrow |00\dots\rangle$ and $|1\rangle \rightarrow |11\dots\rangle$. This is a primitive example of how a single logical qubit can be encoded to multiple physical qubits using quantum error-correcting codes (QECCs). As mentioned in the general derivation and illustrated by the GHZ example above, the many-body entanglement swapping protocol is agnostic to the basic building blocks of the target state, applying equally well for physical qubits as well as blocks of physical qubits encoding a logical qubit. This means that the standard machinery of quantum error correction can be readily accommodated in the protocol, opening the door to fault-tolerant entanglement swapping.

Logical qubits can be encoded using established QECCs, such as stabilizer codes, enabling our protocol to support the sharing of any target state that can be prepared using stabilizer circuits [33, 34]. This includes key classes of entangled states, such as logical Bell pairs and logical cluster states. To further extend the protocol toward fully fault-tolerant entanglement swapping for arbitrary target states (including those requiring non-Clifford operations) QECCs can be combined with magic state distillation techniques [35]. In this broader context, if the generating unitary U is implemented fault-tolerantly, and if Eve performs fault-tolerant projective measurements, then the many-body entanglement swapping protocol can be executed in a fully fault-tolerant manner. While this extension is conceptually straightforward, it presents substantial technical challenges. Compared to single-pair swapping, fault-tolerant implementation requires more advanced error correction techniques and, in long-distance scenarios, efficient handling of multiple flying qubits—an area that has been explored to some extent in previous works [36, 37]. Nonetheless, meeting these challenges would mark a major step forward in building error-resilient distributed quantum systems and scalable quantum networks.

V. SUMMARY AND OUTLOOK

We established a general many-body entanglement swapping protocol that enables two non-signaling parties to share a high-fidelity copy of a generic many-body quantum state, and we demonstrated its proof of principle on actual quantum hardware. In the emerging era of distributed quantum information processing and quan-

tum networks, this protocol provides key functionalities that are difficult or impossible to achieve by other known methods. These include the sharing of complex states with a generic Schmidt spectrum and the implementation of fault-tolerant entanglement swapping. In forthcoming work, we will employ existing quantum hardware to demonstrate further aspects of the protocol, including sharing more complex states [38].

VI. DATA AVAILABILITY

The data supporting the findings of this work are available upon reasonable request.

VII. CODE AVAILABILITY

The codes implementing the calculations in this work are available upon reasonable request.

VIII. AUTHOR CONTRIBUTIONS

S.H. and Y.M. contributed equally to this work. All the authors developed the project together. S.H. implemented the numerical simulations of random circuits. Y.M. carried out quantum simulations and the associated numerical simulations. A.G.M. advised on the implementation and execution of both simulations. The results were analyzed and the manuscript was prepared jointly by the authors.

IX. ACKNOWLEDGEMENTS

A.G.M. and T.O. acknowledge Jane and Aatos Erkko Foundation for financial support. T.O. also acknowledges the Finnish Research Council project 362573.

X. COMPETING INTERESTS

The authors declare no competing interests.

XI. METHODS

A. Simulation details on the quantum processor

To carry out the quantum simulations presented in Fig. 3, we used IBM’s 127-qubit superconducting quantum processor `ibm_brisbane`, accessed via the IBM Quantum cloud platform [29]. This device is based on fixed-frequency transmon qubits arranged in a heavy-hex lattice architecture. The processor exhibits coherence

times typically ranging from 100 to 300 μ s, with single- and two-qubit gate fidelities exceeding 99.9% and 99%, respectively, and median readout error of $\sim 1.7\%$. For benchmarking and validation purposes (data shown in Fig. 3 (c)), we employed IBM’s high-performance simulators available through Qiskit [39]. These simulators realistically emulate IBM Quantum devices by incorporating noise models that account for native gate errors, qubit connectivity, measurement errors, and decoherence.

We utilized two measurement interfaces [39]: the *Sampler* and the *Estimator*. The Sampler executes quantum circuits multiple times to yield bitstring distributions, faithfully capturing raw hardware noise without applying post-processing. In contrast, the Estimator is designed to evaluate expectation values of observables (e.g., Pauli operators) and employs various noise-aware techniques such as measurement optimization, grouping, and error mitigation to produce smoother and more accurate results. To mitigate the effects of noise and decoherence, we implemented two readily available strategies: *Twirled Readout Error eXtinction* (TREX) [40] and *Dynamical Decoupling* (DD) [41–43]. TREX improves the accuracy of measurements by reducing readout errors through probabilistic averaging over symmetrized measurement outcomes, while DD helps preserve quantum coherence during idle periods by applying carefully designed pulse sequences that dynamically refocus qubit states.

The number of measurement shots, denoted by m , was selected to resolve probability differences down to a standard deviation of approximately $\sigma \sim 1\%$. The standard deviation in estimating a probability p is approximated by $\sigma \approx \sqrt{p(1-p)/m}$. To quantify the similarity between the output and target distributions, as the fidelities shown in Fig. 3(d-g), we have adapted Hellinger distance H . Based on this, the fidelity is defined as $F = (1 - H^2)^2$ which measure lies in the interval $[0, 1]$ and is equivalent to the *classical fidelity* F_H , since it coincides with the *quantum state fidelity* for diagonal density matrices. Such classical fidelity between the output state $|\psi_{AB}\rangle$ and the target state $|\psi_T\rangle$ is given by:

$$F_H(|\psi_{AB}\rangle, |\psi_T\rangle) = \left(\sum_i \sqrt{p_i q_i} \right)^2, \quad (10)$$

where p_i and q_i are the probability components of the output and target distributions, respectively.

B. Quantum noise models

To model the noise effects, we adopt the Kraus representation of quantum channels. In this framework, a noisy quantum process acting on a density matrix ρ is described by a completely positive, trace-preserving map \mathcal{E} , which can be expressed as:

$$\mathcal{E}(\rho) = \sum_k E_k \rho E_k^\dagger, \quad (11)$$

where the operators $\{E_k\}$ are known as Kraus operators and satisfy the completeness relation $\sum_k E_k^\dagger E_k = I$. In the following, we provide the explicit forms of the Kraus operators corresponding to different types of quantum errors, which are commonly encountered in quantum devices.

Single-qubit gate error: For single-qubit gate error, we are using a general Pauli channel error (depolarizing channel error) representation that includes X , Y , and Z error simultaneously, which applies Pauli errors X , Y , and Z with certain probabilities:

$$\mathcal{E}_{1Q}(\rho) = p_x X \rho X + p_y Y \rho Y + p_z Z \rho Z + (1 - \sum_{i \in \{x,y,z\}} p_i) \rho \quad (12)$$

where $p_x, p_y, p_z \in [0, 1]$ denote probability of applying X , Y , and Z error, respectively. Hence, The Kraus operators for this channel are:

$$\begin{aligned} E_0 &= \sqrt{p_x} X, & E_1 &= \sqrt{p_y} Y, \\ E_2 &= \sqrt{p_z} Z, & E_3 &= \sqrt{(1 - \sum_{i \in \{x,y,z\}} p_i)} I. \end{aligned} \quad (13)$$

The specific probability of X , Y , and Z errors on single-qubit gates in IBM Quantum devices are not publicly detailed in terms of individual Pauli error components. IBM typically reports overall single-qubit gate error rates, which encompass various error sources, including decoherence and control imperfections. For simulation purposes, it's common to model single-qubit errors using a depolarizing channel, where X , Y , and Z errors are assumed to occur with equal probability. Hence, we can consider the single-qubit gate error as

$$\begin{aligned} \mathcal{E}_{1Q}(\rho) &= \frac{\eta_{1Q}}{4} X \rho X + \frac{\eta_{1Q}}{4} Y \rho Y \\ &\quad + \frac{\eta_{1Q}}{4} Z \rho Z + (1 - \frac{3\eta_{1Q}}{4}) \rho \end{aligned} \quad (14)$$

where $p_x = p_y = p_z = \frac{1}{4} \eta_{1Q}$.

Readout error: For each qubits, the readout error can be implemented using a confusion matrix by applying after quantum circuit execution classically:

$$R = \begin{bmatrix} P(0|0) & P(0|1) \\ P(1|0) & P(1|1) \end{bmatrix} = \begin{bmatrix} 1 - p_{01} & p_{01} \\ p_{10} & 1 - p_{10} \end{bmatrix} \quad (15)$$

where $P(i|j)$ is the probability to read i given true outcome j . Therefore, p_{01} and p_{10} represent the probability of flipping $0 \rightarrow 1$ and $1 \rightarrow 0$, respectively.

Phase- and Amplitude-damping error: The pure dephasing time T_ϕ satisfy the following expression

$$\frac{1}{T_2} = \frac{1}{2T_1} + \frac{1}{T_\phi} \quad (16)$$

where T_1 and T_2 are energy relaxation time and dephasing time, respectively.

Let $\gamma = 1 - e^{-t/T_1}$ be amplitude-damping channel probability, where t is the gate duration time, and Kraus operators are

$$E_0^{AD} = \begin{bmatrix} 1 & 0 \\ 0 & \sqrt{1-\gamma} \end{bmatrix}, \quad E_1^{AD} = \begin{bmatrix} 0 & \sqrt{\gamma} \\ 0 & 0 \end{bmatrix} \quad (17)$$

where γ represents the probability that the qubit decays from $|1\rangle$ to $|0\rangle$.

The phase-damping error describes a noise process that is uniquely quantum mechanical, depicting the loss of quantum information without loss of energy. By considering $\lambda = 1 - e^{-t/T_\phi}$, the Kraus operators are

$$E_0^{PD} = \sqrt{1-\lambda} \cdot I, \quad E_1^{PD} = \sqrt{\lambda} \cdot Z \quad (18)$$

where λ can be interpreted as the probability that a qubit loses quantum information without loss of energy.

The phase- and amplitude-damping error (PAD) can be consider as product of each noises, $\mathcal{E}_{PAD}(\rho) = \mathcal{E}_{PD}(\rho) \cdot \mathcal{E}_{AD}(\rho)$. Which Kraus operators are

$$\begin{aligned} E_0^{PAD} &= E_0^{PD} \cdot E_0^{AD} \\ E_1^{PAD} &= E_1^{PD} \cdot E_1^{AD} \end{aligned} \quad (19)$$

where η_{PAD} denotes the probability of a qubit capturing both energy relaxation (amplitude damping) and loss of quantum coherence (phase damping).

ECR error: For the ECR gate error, similar to the single-qubit gate, we use a general Pauli channel error model, which can be expressed as a tensor product of single-qubit error representations (13),

$$\mathcal{E}_{ecr}(\rho) = \sum_k E_k^{ecr} \rho E_k^{ect\dagger} = \sum_{i,j} (E_i \otimes E_j) \rho (E_i^\dagger \otimes E_j^\dagger), \quad (20)$$

and η_{ecr} represents the effective error probability for the ECR gate, assuming the error contributions from the two input qubits are equal.

[1] J. I. Cirac, P. Zoller, H. J. Kimble, and H. Mabuchi, Quantum state transfer and entanglement distribution among distant nodes in a quantum network, *Phys. Rev. Lett.* **78**, 3221 (1997).
 [2] H. J. Kimble, The quantum internet, *Nature* **453**, 1023 (2008).

[3] M. Żukowski, A. Zeilinger, M. A. Horne, and A. K. Ekert, "event-ready-detectors" bell experiment via entanglement swapping, *Phys. Rev. Lett.* **71**, 4287 (1993).
 [4] T. Jennewein, G. Weihs, J.-W. Pan, and A. Zeilinger, Experimental nonlocality proof of quantum teleportation and entanglement swapping, *Phys. Rev. Lett.* **88**, 017903

- (2001).
- [5] B. Yurke and D. Stoler, Einstein-podolsky-rosen effects from independent particle sources, *Phys. Rev. Lett.* **68**, 1251 (1992).
 - [6] Č. Brukner, M. Aspelmeyer, and A. Zeilinger, Complementarity and information in “delayed-choice for entanglement swapping”, *Found. Phys.* **35**, 1909 (2005).
 - [7] H. de Riedmatten, I. Marcikic, J. A. W. van Houwelingen, W. Tittel, H. Zbinden, and N. Gisin, Long-distance entanglement swapping with photons from separated sources, *Phys. Rev. A* **71**, 050302 (2005).
 - [8] R. Horodecki, P. Horodecki, M. Horodecki, and K. Horodecki, Quantum entanglement, *Rev. Mod. Phys.* **81**, 865 (2009).
 - [9] K. Azuma, S. E. Economou, D. Elkouss, P. Hilaire, L. Jiang, H.-K. Lo, and I. Tzitrin, Quantum repeaters: From quantum networks to the quantum internet, *Rev. Mod. Phys.* **95**, 045006 (2023).
 - [10] S. Bose, V. Vedral, and P. L. Knight, Multiparticle generalization of entanglement swapping, *Phys. Rev. A* **57**, 822 (1998).
 - [11] C.-Y. Lu, T. Yang, and J.-W. Pan, Experimental multiparticle entanglement swapping for quantum networking, *Phys. Rev. Lett.* **103**, 020501 (2009).
 - [12] P. Bej, A. Ghosal, D. Das, A. Roy, and S. Bandyopadhyay, Information-disturbance trade-off in generalized entanglement swapping, *Physical Review A* **102**, 052416 (2020).
 - [13] S. Liu, Y. Lou, Y. Chen, and J. Jing, All-optical entanglement swapping, *Phys. Rev. Lett.* **128**, 060503 (2022).
 - [14] J. Preskill, Quantum computing in the nisq era and beyond, *Quantum* **2**, 79 (2018).
 - [15] D. P. DiVincenzo, The physical implementation of quantum computation, *Fortschr. Phys.* **48**, 771 (2000).
 - [16] A. D. Córcoles, A. Kandala, A. Javadi-Abhari, D. T. McClure, A. W. Cross, K. Temme, P. D. Nation, M. Steffen, and J. M. Gambetta, Challenges and opportunities of near-term quantum computing systems, *Proceedings of the IEEE* **108**, 1338 (2019).
 - [17] I. Georgescu, The divincenzo criteria 20 years on, *Nat. Rev. Phys.* **2**, 666 (2020).
 - [18] J. Preskill, Beyond nisq: The meqaquop machine (2025).
 - [19] S. Bravyi, A. W. Cross, J. M. Gambetta, D. Maslov, P. Rall, and T. J. Yoder, High-threshold and low-overhead fault-tolerant quantum memory, *Nature* **627**, 778 (2024).
 - [20] B. Fauseweh, Quantum many-body simulations on digital quantum computers: State-of-the-art and future challenges, *Nat. Commun.* **15**, 2123 (2024).
 - [21] M. Mohseni, A. Scherer, K. Johnson, O. Wertheim, M. Otten, N. Aadit, Y. Alexeev, K. Bresniker, K. Cam-sari, B. Chapman, *et al.*, How to build a quantum super-computer: Scaling from hundreds to millions of qubits, arXiv:2411.10406 (2025).
 - [22] E. Bäumer, V. Tripathi, D. S. Wang, P. Rall, E. H. Chen, S. Majumder, A. Seif, and Z. K. Mineev, Efficient long-range entanglement using dynamic circuits, *PRX Quantum* **5**, 030339 (2024).
 - [23] E. Bäumer, V. Tripathi, A. Seif, D. Lidar, and D. S. Wang, Quantum fourier transform using dynamic circuits, *Phys. Rev. Lett.* **133**, 150602 (2024).
 - [24] A. Carrera Vazquez, C. Tornow, D. Ristè, S. Woerner, M. Takita, and D. J. Egger, Combining quantum proces-sors with real-time classical communication, *Nature*, 1 (2024).
 - [25] J. Eisert, M. Cramer, and M. B. Plenio, Colloquium: Area laws for the entanglement entropy, *Rev. Mod. Phys.* **82**, 277 (2010).
 - [26] J. I. Cirac, D. Pérez-García, N. Schuch, and F. Verstraete, Matrix product states and projected entangled pair states: Concepts, symmetries, theorems, *Rev. Mod. Phys.* **93**, 045003 (2021).
 - [27] Z.-Y. Wei, D. Malz, and J. I. Cirac, Sequential generation of projected entangled-pair states, *Phys. Rev. Lett.* **128**, 010607 (2022).
 - [28] X. Chen, A. Dua, M. Hermele, D. T. Stephen, N. Tantivasadakarn, R. Vanhove, and J.-Y. Zhao, Sequential quantum circuits as maps between gapped phases, *Phys. Rev. B* **109**, 075116 (2024).
 - [29] IBM Quantum, *ibm.brisbane* backend, IBM Quantum Platform, <https://quantum-computing.ibm.com> (2025), accessed: 2025-06-25.
 - [30] A. Nahum, J. Ruhman, S. Vijay, and J. Haah, Quantum entanglement growth under random unitary dynamics, *Phys. Rev. X* **7**, 031016 (2017).
 - [31] M. P. Fisher, V. Khemani, A. Nahum, and S. Vijay, Random quantum circuits, *Annual Review of Condensed Matter Physics* **14**, 335 (2023).
 - [32] J. M. Koh, S.-N. Sun, M. Motta, and A. J. Minnich, Measurement-induced entanglement phase transition on a superconducting quantum processor with mid-circuit readout, *Nat. Phys.* **19**, 1314 (2023).
 - [33] B. M. Terhal, Quantum error correction for quantum memories, *Rev. Mod. Phys.* **87**, 307 (2015).
 - [34] R. Acharya, D. A. Abanin, L. Aghababaie-Beni, I. Aleiner, T. I. Andersen, M. Ansmann, F. Arute, K. Arya, A. Asfaw, N. Astrakhantsev, *et al.*, Quantum error correction below the surface code threshold, *Nature* **638**, 920 (2024).
 - [35] D. Litinski, Magic State Distillation: Not as Costly as You Think, *Quantum* **3**, 205 (2019).
 - [36] N. H. Nickerson, Y. Li, and S. C. Benjamin, Topological quantum computing with a very noisy network and local error rates approaching one percent, *Nature communica-tions* **4**, 1756 (2013).
 - [37] S. Muralidharan, L. Li, J. Kim, N. Lütkenhaus, M. D. Lukin, and L. Jiang, Optimal architectures for long distance quantum communication, *Scientific reports* **6**, 20463 (2016).
 - [38] Y. Mafi, A. G. Moghaddam and T. Ojanen, in prepara-tion.
 - [39] A. Javadi-Abhari, M. Treinish, K. Krsulich, C. J. Wood, J. Lishman, J. Gacon, S. Martiel, P. D. Nation, L. S. Bishop, A. W. Cross, *et al.*, Quantum computing with qiskit, Preprint at <https://arxiv.org/abs/2405.08810> (2024), accessed June 2025.
 - [40] E. Van Den Berg, Z. K. Mineev, and K. Temme, Model-free readout-error mitigation for quantum expectation values, *Phys. Rev. A* **105**, 032620 (2022).
 - [41] L. Viola and S. Lloyd, Dynamical suppression of decoherence in two-state quantum systems, *Phys. Rev. A* **58**, 2733 (1998).
 - [42] L. Viola, E. Knill, and S. Lloyd, Dynamical decoupling of open quantum systems, *Phys. Rev. Lett.* **82**, 2417 (1999).
 - [43] L.-M. Duan and G.-C. Guo, Suppressing environmen-tal noise in quantum computation through pulse control, *Phys. Lett. A* **261**, 139 (1999).